

Appendix: Analytical Techniques

Chromium isotope analyses

Chromium isotopic analyses were completed on three different sample aliquots: small internal fragments of AhS 91A and AhS 671 and an aliquot extracted from clast #28 found within NWA 10657. The fragments of AhS 91A and AhS 671 were visually inspected to ensure no visible fusion crust or terrestrial weathering product was present on the fragment to be processed and then were crushed and homogenized using an agate mortar and pestle. For clast #28 of NWA 10657, optical microscopy was used to visualize the clast (Fig. S1) and identify material for extraction. Small pieces of the internal portion of the clast were extracted using a metal dental tool, ensuring that no matrix material was adhered, by minimizing material from the outer edge of the clast. A small fragment was taken for Cr isotopic measurements, while material from the same clast was reserved for oxygen and petrographic analyses. Following extraction, the fragment from clast #28 was also crushed and homogenized using an agate mortar and pestle. The resulting sample powders of AhS 91A (24.77 mg), AhS 671 (10.84 mg), and clast #28 of NWA 10657 (3.16 mg) were transferred to individual PTFE Parr capsules along with a 3:1 mixture of concentrated HF and HNO₃. The PTFE capsules were sealed in stainless steel jackets and heated in a 190°C oven for 96 hours to ensure complete dissolution of silicate and refractory phases. After complete dissolution, the samples were processed through a 3-column ion chromatography separation procedure as described in Yamakawa et al. (2009). The isotopic compositions of the purified Cr fractions were analyzed using a Thermo *Triton Plus* thermal ionization mass spectrometer at the University of California, Davis. Details of the mass spectrometry procedure are given in Sanborn et al. (2019). All Cr isotopic data are reported as parts per 10,000 deviation (ϵ -notation) from the terrestrial composition as represented by NIST SRM 979 analyzed in the same analytical session.

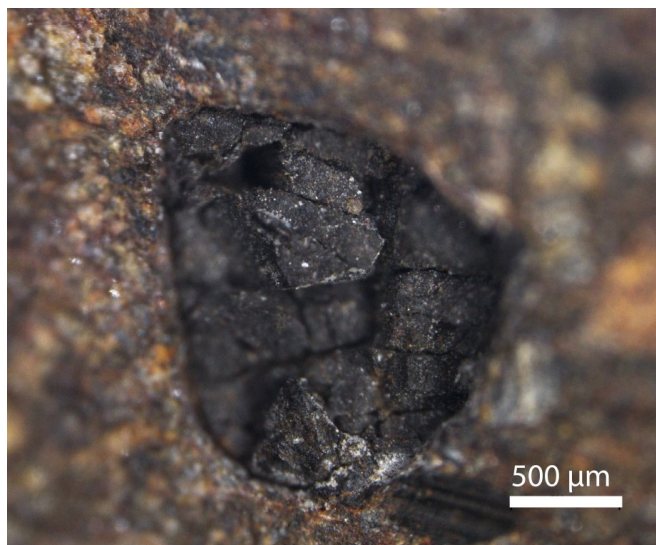


Figure S1. NWA 10657 clast 28 on surface of slab. Optical photomicrograph.

Oxygen isotope analyses

Oxygen isotope data for AhS 91A and AhS 671 were reported in Goodrich et al. (2019a). Analytical techniques used here for NWA 10657 clast 28 were the same as described in that paper.

Hydrogen isotope analyses

Hydrogen isotope analysis was performed with the Cameca 1280 ion microprobe equipped with a Hyperion II RF plasma ion source at University of Hawai'i, Manoa. A $^{16}\text{O}^-$ primary beam accelerated to -13keV was set to ~4 nA and defocused to ~30 μm . Positive secondary ions of hydrogen isotopes, $^{12}\text{C}^+$, $^{24}\text{Mg}^{2+}$, and $^{30}\text{Si}^+$ were measured in mono-collection mode with an electron multiplier. A field aperture gating was selected to collect secondary ions only from a ~4 \times 4 μm area in the center of the beam, excluding H ions from beam crater edges. A mass resolving power of ~2000 effectively resolved signals from D^+ and H_2^+ . Measurements consisted of 20 cycles and H^+ , D^+ , $^{12}\text{C}^+$, $^{24}\text{Mg}^{2+}$, and $^{30}\text{Si}^+$ were measured each cycle for 3s, 40s, 1s, 1s, and 1s, respectively. During 500s of pre-sputtering, we imaged H^+ with the field aperture opened, allowing us to observe H distribution over the entire 30 μm region being sputtered. Small adjustments to the beam position were made in order to avoid anhydrous grains in matrix and to center the beam on H-rich areas. These fine-grained phyllosilicate “packets” were measured in the matrices of all samples. Coarse-grained phyllosilicates devoid of anhydrous phases were measured in AhS 671-03 and AhS 91A. Time interpolation was performed to correct for mono-collection and dead-time corrections were applied assuming an electron multiplier deadtime of 30ns. A terrestrial chrysotile standard characterized by Alt and Shanks (2006) was selected to determine the instrumental mass fractionation (IMF) of H isotopes. The standard was measured three times before and after the sample measurements each day in order to monitor IMF drift. All samples except NWA 10657 clast 2 were measured in the same session and the IMF was not observed to drift during this session. We therefore averaged 43 standard measurements to determine the IMF for the first session. NWA 10657 clast 2 was measured in a different session and the IMF was determined from the average of six standard measurements. Reported errors for each measurement are the greater of the standard error calculated from the individual cycles and the statistical counting error after summing the counts from all cycles.

In the matrices of CCs fine-grained phyllosilicates are intergrown with D-rich organic materials at the sub-micron scale (Le Guillou and Brearley 2013; Le Guillou et al. 2014) and phyllosilicates cannot be exclusively targeted with the current method. However, primary $^{16}\text{O}^-$ ions ionize H in phyllosilicates ~330-500x more efficiently than H in organics (Deloule and Robert 1995; Bonal et al. 2010). We also note that in C1 and C2 lithologies, phyllosilicates are much more abundant than organics, so our D/H measurements primarily reflect the composition of structurally bound hydroxyl and interlayer H_2O in phyllosilicates.

Several procedures were carried out to minimize contamination from terrestrial H. The sample chamber was baked prior to measurements and pumped down to $\leq 10^{-10}$ torr with LN_2 cold trap in the sample chamber. Samples were stored in a vacuum oven at ~58°C for at least three days to allow adsorbed water to dissipate and then immediately transferred to the ion probe's airlock chamber, where they remained overnight to facilitate outgassing of the epoxy embedding medium. After the initial standard measurements, the samples were loaded into the sample chamber and measurements did not commence until the vacuum again reached $\leq 10^{-10}$ torr. Our pre-sputtering time (500s) removed the vast majority of the C-coating, except for residual C that infiltrated small cracks and pore spaces. Residual C remaining after the pre-sputter was easily identified in plots of

$^{12}\text{C}/\text{H}$ vs. cycle number, when the $^{12}\text{C}/\text{H}$ ratio was observed to decrease exponentially over the first few cycles before reaching a constant value. In this case, the first cycles with decreasing $^{12}\text{C}/\text{H}$ were eliminated from calculations of D/H, ensuring that terrestrial H bound to the C coating was not included in our calculations.

Scanning Electron Microscopy (SEM) and Electron Microprobe Analysis (EMPA)

Petrologic data for AhS 91A and AhS 671 were reported in Goodrich et al. (2019a). Analytical methods used here for NWA 10657 were the same as described in that paper.